This ms is similar to Magnetic Resonance in Medicine 44:427-432 (2000)

Apparent diffusion coefficient and MR relaxation during osmotic manipulation in isolated turtle cerebellum

Jacqueline M. O'Shea, Stephen R. Williams, Nick van Bruggen, Anthony R. Gardner-Medwin

From the Royal College of Surgeons Unit of Biophysics, Institute of Child Health, University College London, 30 Guilford Street, London WC1N 1EH, UK. (J.M.O'S., S.R.W., N.v.B.) and Dept. Physiology, University College London, London. WC1E 6BT (J.M.O'S., A.R.G.M.).

Running title: ADC and cell volume in vitro

Address correspondence to: Dr. A.R. Gardner-Medwin, Dept. of Physiology, UCL, London WC1E 6BT, UK
Email: ucgbarg@ucl.ac.uk *Phone* +44 (020) 7380 7135, *FAX* +44 (020) 7383 7005

ABSTRACT

The apparent diffusion coefficient (ADC) and relaxation times of water were measured by magnetic resonance imaging (MRI) in the isolated turtle cerebellum during osmotic cell volume manipulation. The aim was to study effects of cell volume changes, a factor in ischaemia and spreading depression, in isolation from considerations of blood flow and metabolism. Cerebella were superfused at 12-14°C with solutions ranging from 50-200% normal osmolarity. Hypotonic solutions, which are known to cause cell swelling, led to reductions of ADC and increases of T2 while hypertonic solutions had opposite effects. This supports the concept that ADC varies with the extracellular space fraction and, combined with published data on extracellular ion diffusion, is consistent with fast or slow exchange models with effective diffusion coefficients that are approximately 1.7 times lower in intracellular than extracellular space. Spin-spin relaxation can be affected by osmotic disturbance, though such changes are not seen in all pathologies that cause cell swelling.

Key words*:* diffusion (ADC), tortuosity, cell volume, osmotic manipulation

INTRODUCTION

Magnetic Resonance (MR) diffusion weighted imaging (DWI) provides non-invasive measurements of the apparent diffusion coefficient (ADC) of water (1), which have been shown to decrease during the acute stage of cerebral ischaemia. Changes have been seen on many time scales (2-8) and may be indicative of both irreversible and transient pathologies, including cortical spreading depression (9, 10). The potential to apply the technology in the clinical setting for diagnosis and monitoring of acute stroke in patients is now being realised - for a recent discussion and review see Baird and Warach (2). Despite these applications, understanding of the biophysical mechanisms of the ADC changes remains incomplete.

An increasing body of evidence implicates cell volume change in the observed ADC changes *in vivo* (11-14) and *in vitro* (15-17). These models however are complicated by haemodynamic effects or possible metabolic compromise and lack of control of the cell volume changes. The

turtle cerebellum is a good preparation for studying the relationship between cell volume and ADC changes. It is structurally well described (18,19), the biochemical basis of its remarkable anoxia resistance is well documented (20,21 and references therein), and its extracellular volume fraction has been extensively measured in response to osmotic challenges (22). This study examines the effect of similar challenges affecting cellular and extracellular volume under controlled conditions on MR parameters, particularly the ADC and T2 relaxation. A brief report of preliminary studies has been published (23).

METHODS

Tissue

American pond turtles (*Pseudomys scripta elegans* and *Chrysemys picta*, 400 - 600g, shell length 12 - 16 cm) were decapitated and the head cooled in ice for 3 min before excision and dissection of the brain under cold oxygenated phosphate buffer (NaCl 140 mM, KCl 3mM, NaH_2PO_4 2 mM, Na_2HPO_4 4 mM, $CaCl_2$ 1mM, glucose 20 mM, saturated with 100% O_2 ; pH 7.5). The dura and choroid plexus were dissected away and the cerebellum was separated by cutting the cerebellar peduncles. It was then stored on ice in a sealed 2.5 ml eppendorf tube containing the same oxygenated buffer for up to one hour (transport and preparation time) before transfer to the recording chamber, where perfusion was maintained initially with the control solution for experiments, equilibrated with 95% O_2 + 5% CO_2: NaCl 115mM, KCl 5 mM, $NaHCO_3$ 25 mM, $CaCl_2$ 3.5 mM, $MgCl_2$ 3.5 mM, glucose 20mM; pH 7.4 -7.6. Subsequent changes to solutions with different osmolarity, obtained by omission or addition of NaCl, were made for periods of at least 45min, followed by return to the control solution. The range of nominal osmolarities (summed molar concentrations of ionic species) was from 171 to 781 mosmol.l^{-1}, with the control solution 331 mosmol.l^{-1}. This corresponds to effective osmolalities determined by freezing point depression of approximately 0.16-0.68 osmol.kg^{-1} (22).

The tissue was held between horizontal layers of thin cotton cloth (20 x 8 mm) suspended in a chamber (20 x 10 x 10 mm) containing the 95% O_2 + 5% CO_2 gas mixture. The cloths were saturated with flowing saline fed to one end at 150 µl.min^{-1} . Fluid movement (observed with a tracer dye) was fairly uniform and laminar at ca. 0.5 mm.s^{-1}. Waste solution was removed at the far end by suction through a piece of sponge. A second suction line removed any fluid accumulated at the bottom of the recording chamber. Twin feed pipes permitted rapid solution changes to be made from outside the magnet, which affected the tissue abruptly after about 20s as detected by Ag/AgCl electrodes embedded in the cloth beside the tissue.

Solutions were bubbled at ca. 10^o C near the peristaltic pump, 3m from the magnet. They were near room temperature by the time they entered the magnet where they were recooled and equilibrated with the gas by passing through a 80 mm length of 1mm (internal diameter) silicone rubber tubing (relatively gas-permeable) within the pipe carrying gas to the chamber, which was itself surrounded by the returning cooling water. The final connection to the inner chamber (Fig. 1) was via 1 mm diameter Teflon (PTFE) pipe, relatively impermeable to gases. Observations with O_2 electrodes showed that the design provided nearly full O_2 equilibration of the fluid surrounding the tissue at normal flow rates. The good metabolic provision to the tissue was further verified by its ability to sustain multiple waves of spreading depression under these conditions, for over 24 hours.

The chamber was inserted in a 2.35 T horizontal bore magnet (Oxford Instruments, Oxford,

UK) interfaced to a SMIS (Surrey Medical Information Systems, UK) console. The magnet was fitted with 12 cm inner diameter homemade gradient coils, capable of up to 250 $mT.m^{-1}$ output over ± 20 mm from the gradient centre. A 70 mm cylindrical transmit coil aligned along the bore of the magnet was used for RF excitation pulses with a 2-turn 6 mm diameter coil in the tissue chamber for detection (Fig. 1). The coils were tuned at 100 MHz and decoupled using crossed diodes.

MR Protocols

For most of the experiments reported here a double echo sequence was employed (Fig. 2), with echoes at 80ms and 160ms to provide estimates of T2. Versions of this with and without the diffusion-weighting gradient pulses G1, G2 were interleaved and thus provided estimates of the apparent diffusion coefficient for excited protons. Thus four images were obtained for every complete acquisition cycle, which lasted 130s. These sets of images were usually obtained continuously throughout the period before, during and after solution changes. The critical MR parameters were as follows: TR 2000 ms; 2 averages; 16 -phase encoding steps; slice thickness 2 mm; slice select direction perpendicular to the principal tissue plane (y-axis: Fig.1); FOV 20-30 mm; gradient strength (G_d) 54.2 $mT.m^{-1}$; δ = 16.1 ms; Δ = 32 ms, diffusion gradient ramp 1 ms. The effective diffusion time $T_{diff} = (\Delta - \delta/3)$ was 27 ms and the diffusion weighting factor due to G1 and G2, $b = \gamma^2 G_d^2 \delta^2 (\Delta - \delta/3)$ was 1454 $s.mm^{-2}$ along either x- or y-axes (Fig. 1). The non diffusion-weighted images had a small diffusion weighting of 3.7 $s.mm^{-2}$.

ADC and T2 were estimated from the ratios of signal intensities:

$$ADC = \ln (S0/S1) / (b1 - b0) \qquad [1]$$

where S1 = signal intensity of the DW-image, S0 = signal intensity of the equivalent non DW-image; b1 = 1454 $s.mm^{-2}$, b0 = 4 $s.mm^{-2}$. T2 was estimated from the ratio of the two image intensities derived from a single double echo sequence:

$$T2 \ (ms) = 80 / \ln(S_{80} / S_{160}) \qquad [2]$$

The log ratio in equation 1 could be calculated for either the 80 ms or 160 ms echoes, but the differences were no more than a few percent and were unaffected by the solution changes. Similarly, T2 could be calculated (equation 2) for signals with or without diffusion weighting and did not differ significantly. The results presented here are those for ADC estimates from the 80ms echoes and T2 estimates without diffusion-weighting. Measurements with a phantom consisting of a glass bulb filled with 20% albumin solution within the chamber gave ADC = 17.4×10^{-4} $mm^2.s^{-1}$ and T2 = 107 ms. Changes due to osmolarity differences at the tissue are expressed relative to prior measurements in control saline (331 $mosmol.l^{-1}$), averaged over at least four sets of images (8 min).

In initial experiments, single echo sequences (interleaved with and without diffusion weighting along the y-axis) were employed with TE either 80ms or 160ms. The results suggested that there might be T2 as well as ADC changes, and led to implementation of the double-echo sequence. Fig. 3 shows a 2-D image of a cerebellum with the 6 x 6 pixel (approx. 3x3 mm) region of interest (ROI) indicated, as used for signal measurements.

RESULTS

Initial measurements of ADC in fresh tissue, with osmolarity=331 mosmol.l^{-1}, averaged 3.88 ± 0.24 (s.e.m.) $\times 10^{-4}$ $mm^2.s^{-1}$ (n=13: number of preparations) with gradients along the y-axis perpendicular to the plane of the tissue and 4.75 ± 0.19 $\times 10^{-4}$ $mm^2.s^{-1}$ (n=31) along the x-axis parallel to the tissue. These observations are significantly different ($P<0.01$, rank sum test) but since for technical reasons they could not both be made in a single preparation and the data derive from separate experimental series, we cannot be sure whether the small (20%) difference is due to tissue anisotropy or other factors. The overall mean of 73 ADC measurements under baseline conditions in the 44 tissue preparations (including measurements following re-equilibration after interventions) was 4.69 ± 0.13 (s.e.m.)$\times 10^{-4}$ $mm^2.s^{-1}$. The corresponding T2 measurements averaged 77.8 ms (± 1.3 ms s.e.m., n=73) .

Equilibration with altered solutions was observed with exposures for 45-90 minutes, followed by return to control saline. Hypotonic solutions, which induce swelling of both the cells and the tissue as a whole (22), caused ADC to fall, and T2 and signal intensity S_{80} (with TE=80 ms) to rise (Fig. 4A). Opposite changes were seen with raised osmolarity (Fig. 4B). The changes started to be evident in the first or second image cycle after solution change (ca. 2min/cycle) and approached steady state levels with time constants of up to 30 min in the extreme hypotonic solution (Fig. 4A). The ADC changes were proportionately larger than the T2 changes, especially with hyperosmolar interventions, and developed with a faster timecourse than either T2 or S_{80}.

On return to control solutions the ADC changes often overshot the baseline at a time when the signal intensity and T2 values had not yet recovered to baseline levels. This overshoot might be due to adaptation of cells to the altered environment, though such regulation of cell volume has not been clearly evident in this preparation (22). It may alternatively be due to long-lasting residual swelling of tissue in deep layers following hypotonic exposure, that will tend to stretch apart the superficial tissue in which the cells will re-equilibrate more rapidly to normal volume. This could cause an abnormal elevation of extracellular space fraction and ADC, in part of the tissue, before the tissue water content and T2 have returned to baseline. In hyperosmotic Ringer the time course of the changes of ADC and T2 were faster (Fig. 4B), presumably because the larger extracellular volume fraction under these conditions leads to faster diffusional equilibration.

Steady state percentage changes in ADC and T2 relative to control levels were estimated from the individual timecourses, and are plotted in Fig. 5 as functions of osmolarity. The largest changes were in ADC, averaging -38% and +39% for approximately 2-fold changes of osmolarity to 171 and 781 mosmol.l^{-1}. The T2 changes averaged +27% and -11% under the same conditions. Means (±1 s.e.m., based on the indicated numbers of observations) are shown on Fig. 5. A conspicuous feature of the data was that the changes of T2 were much smaller in the hyper- than hypo-osmotic solutions. The changes in signal intensity (S_{80}) shown in Fig. 4 are, for the sake of clarity, not shown in Fig. 5. They averaged typically +26% and -27% for the hypo- and hyper-osmotic interventions, but their interpretation would be complex because they will have been affected by factors that include the T2 changes and net changes of total tissue volume (uptake and loss of water).

The changes shown in Fig. 5 are distinguished for the experiments with diffusion gradients along the x- and y-axes, parallel (squares) and perpendicular (diamonds) to the plane of the tissue. The ADC changes with the extreme hypo-osmotic intervention were significantly greater when measured in the plane of the tissue (-44.1% ± 1.7% s.e.m., n=29) than

perpendicular (-30.0% ± 1.9% s.e.m., n=17 perpendicular; t=5.4, P<0.0001). In these experiments the mean ADC measurements were initially 12% higher measured along the x-axis under baseline conditions (4.8 vs. 4.3 $\times 10^{-4}$ $mm^2.s^{-1}$) and became 10% lower along the x-axis under the hypo-osmotic conditions (2.7 vs. 3.0 $\times 10^{-4}$ $mm^2.s^{-1}$). These differences between the two experimental series are too small to be confidently related to tissue anisotropy.

DISCUSSION

The principal aim of these experiments was to study ADC in relation to controlled disturbances of the osmolarity of the cell environment, which cause cell swelling and shrinkage. Since there are data available for the extracellular volume fraction in this tissue under similar conditions (22) it is possible to relate the observed changes directly to the relative volumes of the intracellular and extracellular compartments (Fig. 6). The data for the absolute ADC values corresponding to Fig. 5 are plotted in Fig. 6 against the extracellular volume fraction V_{EC} inferred for equivalent osmolarities from the measurements of Krizaj et al. (22) with ion selective microelectrodes and TMA^+ iontophoresis. The relationship is fairly well fitted over the data range (V_{EC}=0.1-0.6) by a number of models (lines 1-4) described below.

The relationship between ADC and cell volume fraction can be interpreted in relation to either a fast or slow exchange model for interaction between the two compartments. A simple fast exchange model, due to Benveniste (11), has received considerable attention as a proposed mechanism to explain ADC decreases during cerebral ischaemia (11,13,14,24). Exchange is assumed fast enough, compared with the diffusion time (27ms in our experiments) that displacements of water molecules represent statistically averaged diffusion fluxes in IC and EC compartments, with their diffusion coefficients weighted according to volume:

$$ADC = V_{EC}(ADC_{EC}) + V_{IC}(ADC_{IC}) \qquad [3]$$

V_{EC} and V_{IC} are the fractional volumes of extracellular (EC) and intracellular (IC) space such that $V_{IC} + V_{EC} = 1$. The linear relation between ADC and V_{EC} means that the coefficients can be estimated from a linear regression (line 1) in Fig. 6, giving $ADC_{EC} = 9.6 \times 10^{-4}$ $mm^2.s^{-1}$ and $ADC_{IC} = 2.8 \times 10^{-4}$ $mm^2.s^{-1}$, with a ratio 3.5:1. Since the regressions for the x-axis and y-axis data contributing to Fig. 6 were not significantly different, the data were pooled.

There are data to show that the effective diffusion coefficient of ions in EC space is not constant under conditions with cell swelling and shrinkage (22). The reduction of diffusion coefficient for a substance restricted to either the EC or IC compartment, relative to diffusion in free water ($D_0 = 17.2 \times 10^{-4}$ $mm^2.s^{-1}$ for protons at 14°C (25)), is usually expressed as a tortuosity factor λ^2. Thus the full equation becomes:

$$ADC = V_{EC}\, D_0\, \lambda_{EC}^{-2} + V_{IC}\, D_0\, \lambda_{IC}^{-2} \qquad [4]$$

In simple situations λ is the factor by which diffusion path lengths are increased by obstructions in the compartment, but λ is also raised by viscosity, molecular interactions and varicosities in the tissue space. Krizaj et al. (22) measured both λ_{EC} and V_{EC} for ionic diffusion in turtle cerebellum, finding λ_{EC} to vary from 1.8-1.5 over the range V_{EC}=0.1-0.8 when osmolarity was changed. We can therefore calculate the first term in equation 4 on the assumption that λ_{EC} has similar values for protons and extracellular ions (Fig. 6, line 5). Extracellular diffusion accounts for only about a third of the observed ADC under normal conditions (V_{EC}=0.22) but it varies steeply with changes of V_{EC}. There are no comparable data

for IC tortuosity, but a constant value $\lambda_{IC} = 2.2$ combined with the EC data gives a reasonable fit (Fig. 6, line 3, with the IC component shown separately as line 6). The significant deviation from the data at low V_{EC} could be eliminated by supposing that λ_{IC} rises as the cells swell, to about 2.4, which is plausible if cells swell preferentially in regions where membrane and fibrillary structural constraints are weakest, and consistent with MR measurements (26) of diffusion of IC 2-fluoro-2-deoxyglucose-6-phosphate (2FDG-6P) in ischaemia. The inferred ratio of EC and IC diffusion coefficients ($\lambda_{IC}^2 : \lambda_{EC}^2$) at normal osmolarity is 1.7:1. This is substantially smaller, and presumably more accurate, than the ratio (3.5:1) for $ADC_{EC} : ADC_{IC}$ estimated from the fit obtained above on the assumption that both parameters are constant. Both ratios are much smaller than the value 23:1 inferred by Benveniste et al. for the rat brain (11), which was based on an IC diffusion coefficient that was probably low for brain tissue (24) and an EC coefficient that was too high (equivalent to $\lambda_{EC} = 1$). They differ from the approximately 1:1 ratio for EC and IC diffusion coefficients of 2FDG-6P estimated by Duong et al. [26]. Differences between the behaviour of protons and 2FDG-6P may not be surprising, however, since they will have different distributions and binding profiles within the various cell compartments and between different cell types in brain tissue.

Although a fast exchange model provides a reasonable interpretation of the relationship between ADC and cell volume fraction, the data in Fig. 6 may also be fitted without the fast exchange assumption. A slow exchange model, in which EC and IC water contribute to the signals independently while diffusing within their own compartments with characteristic EC and IC diffusion coefficients, leads to a non-linear combination of the coefficients because it is the attenuated signal intensities that now add, rather than the diffusion fluxes:

$$ADC = - \ln(V_{EC} e^{-b.ADC_{EC}} + V_{IC} e^{-b.ADC_{IC}}) b^{-1} \qquad [5]$$

Line 2 in Fig. 6 shows the result of fitting this equation to the data with fixed coefficients: $ADC_{EC} = 12\times10^{-4}$ mm^2.s^{-1} and $ADC_{IC} = 2.8\times10^{-4}$ mm^2.s^{-1}. The line does not differ markedly from the linear regression within the range of the data. A probably more accurate analysis again involves expanding $ADC_{EC} = D_0 \lambda_{EC}^{-2}$ in equation 5 and employing the known values of λ_{EC} (22) over the range V_{EC}=0.1-0.6. Assuming the same fixed value for IC tortuosity as for the fast exchange model ($\lambda_{IC} = 2.2$) we obtain only a slightly less good prediction, as shown by line 4. As with the fast exchange model, variations of λ_{IC} with cell volume (from approximately 1.9 at V_{EC}=0.6 to 2.4 at V_{EC}=0.1) can generate a good fit. Thus, though the data are consistent with a fast exchange model, they do not favour it over a slow exchange model. Both models require an assumption that proton diffusion within the cells is approximately 1.7 times slower than outside. The true situation must of course be intermediate between extreme slow and fast exchange models, with time constants yet to be inferred.

We observed a substantial increase of T2 with hypotonic solutions, though only a small reduction in hypertonic solutions (Fig. 5). Cell swelling due to ischaemia in mammalian brain is not usually associated with increases of T2, and indeed small decreases have been seen in the gerbil with global cerebral ischaemia (27) and in the rat with hypoxia measured at high field strengths (28,29); both types of observation were attributed to altered blood oxygenation, which is not a factor in our experiments. Our conditions do differ from ischemia in that the cell swelling is caused by a reduction of osmolarity rather than metabolic insufficency, and significant changes of total tissue water content are induced (22). Other hypotonic interventions have also led to T2 increases, in isolated *Aplysia* neurons (30) and with prolonged plasma hypotonicity (and effectively regulated brain water content) in rabbits *in vivo* (31). It is not yet clear how tissue water content, cell volume and osmolyte regulation interact to affect T2 (31),

but in our experiments it is noteworthy that the T2 changes are similar in magnitude (and in the asymmetry of their behaviour to hypo- and hyper-tonic interventions) to the changes of total water content inferred by Krizaj et al. (22: their Fig. 4).

Cell swelling is a feature of several CNS pathologies in which DW-image changes and ADC changes have been observed. Our experiments, coupled with previous physiological studies (22), serve to identify the quantitative relationship between ADC and cell volume in a relatively simple situation and to show that it is consistent with simple models, with plausible parameters of EC and IC diffusion applied to MR data. The significance of the changes of spin-spin relaxation (T2) remains to be elucidated.

ACKNOWLEDGMENTS

We thank C. Nicholson for providing data prior to publication and J. Houseman for technical assistance. Grant support was from the Medical Research Council, Royal Society and Wellcome Trust.

REFERENCES

1. Le Bihan D, Breton E, Lallemand D, Grenier P, Cabanis E, Laval-Jeantet M. MR imaging of intravoxel incoherent motions: application to diffusion and perfusion in neurologic disorders. Radiology 161, 401-7 (1986).

2. Baird AE, Warach S. Magnetic resonance imaging of acute stroke. J. Cereb. Blood Flow Metab. 18, 583-609 (1998).

3. Busza AL, Allen KL, King MD, van Bruggen N, Williams SR, Gadian DG. Diffusion-weighted imaging studies of cerebral ischemia in gerbils: potential relevance to energy failure. Stroke 23, 1602-12 (1992) .

4. Dardzinski BJ, Sotak CH, Fisher M, Hasegawa Y, Li L, Minematsu K. Apparent diffusion coefficient mapping of experimental focal cerebral ischemia using diffusion-weighted echo-planar imaging. Magn. Reson. Med. 30, 318-25 (1993) .

5. Davis D, Ulatowski J, Eleff S, Izuta M, Mori S, Shungu D, van Zijl PCM. Rapid monitoring of changes in water diffusion coefficients during reversible ischemia in cat and rat brain. Magn. Reson. Med. 31, 454-60 (1994).

6. Warach S, Chien D, Li W, Ronthal M, Edelman RR. Fast magnetic resonance diffusion-weighted imaging of acute human stroke. Neurology 42, 1717-23 (1992).

7. Yongbi MN, Huang NC, Branch CA, Helpern JA. The application of diffusion-weighted line-scanning for the rapid assessment of water ADC changes in stroke at high magnetic fields. NMR Biomed. 10, 79-86 (1997).

8. Decanniere C, Eleff S, Davis D, van Zijl PCM. Correlation of rapid changes in the average water diffusion constant and the concentration of lactate and ATP breakdown products during global ischemia in cat brain. Magn. Reson. Med. 34, 343-52 (1995).

9. Gardner-Medwin AR, van Bruggen N, Williams SR, Ahier RG. Magnetic Resonance Imaging of propagating waves of spreading depression in the anesthetized rat. J. Cereb. Blood Flow Metab. 14, 7-11 (1994).

10. Latour LL, Hasegawa Y, Formato JE, Fisher M, Sotak CH. Spreading waves of decreased diffusion coefficient after cortical stimulation in the rat brain. Magn. Reson. Med. 32, 189-98 (1995).

11. Benveniste H, Hedlund LW, Johnson GA. Mechanism of detection of acute cerebral ischemia in rats by diffusion-weighted magnetic resonance microscopy. Stroke 23, 746-54 (1992).

12. Hasegawa Y, Formato JE, Latour LL, Gutierrez JA, Liu KF, Garcia JH, Sotak CH, Fisher M. Severe transient hypoglycemia causes reversible change in the apparent diffusion of water. Stroke 27, 1648-56 (1996).

13. Sevick RJ, Kanda F, Mintorovitch J, Arieff AI, Kucharczyk J, Tsuruda JS, Norman D, Moseley ME. Cytotoxic brain edema: assessment with diffusion-weighted MR imaging. Radiology 185, 687-90 (1992).

14. van Gelderen P, de Vleeschouwer MHM, DesPres D, Pekar J, van Zijl PCM, Moonen CTW. Water diffusion and acute stroke. Magn. Reson. Med. 31, 154-63 (1994).

15. Anderson AW, Zhong J, Petroff OAC, Szafer A, Ransom BR, Prichard JW, Gore JC. Effects of osmotically driven cell volume changes on diffusion-weighted imaging of the rat optic nerve. Magn. Reson. Med. 35, 162-7 (1996).

16. Flogel U, Niendorf T, Serkowa N, Brand A, Henke J, Leibfritz D. Changes in organic solutes, volume, energy state, and metabolism associated with osmotic stress in a glial cell line: a multinuclear study. Neurochem. Res. 20(7), 793-802 (1995).

17. Buckley DL, Bui JD, Phillips MI, Zelles T, Inglis BA, Plant HD, Blackband SJ. The effect of ouabain on water diffusion in the rat hippocampal slice measured by high resolution NMR imaging. Magn. Reson. Med. 41, 137-42 (1999).

18. Mugnaini E, Atluri RL, Houk JC. Fine structure of granular layer in turtle cerebellum with emphasis on large glomeruli. J. Neurophysiol. 37, 1-29 (1974).

19. ten Donkelaar HJ, Bangma GC. The Cerebellum. In: Gans C, Northcutt RG, Ulinski PS, editors. Biology of the Reptilia. London: Academic Press; 1979. p 496-586.

20. Hochachka PW, Land SC, Buck LT. Oxygen sensing and signal transduction in metabolic defense against hypoxia: lessons from vertebrate facultative anaerobes. Comp. Biochem. Phys A 118(1), 23-9 (1997).

21. Lutz PL. Mechanisms for anoxic survival in the vertebrate brain. Ann. Rev. Physiol. 54, 619-37 (1992).

22. Krizaj D, Rice ME, Wardle RA, Nicholson C. Water compartmentalization and extracellular tortuosity after osmotic changes in cerebellum of *Trachemys scripta*. J. Physiol. 492, 887-96 (1996).

23. O'Shea J, van Bruggen N, Gardner-Medwin AR, Williams SR. An isolated preparation for studying the relationship between cell volume and diffusion weighted imaging signal intensity changes. In: "Proc., ISMRM, 3rd Annual Meeting, Nice, France, 1995", p. 30.

24. Helpern JA, Ordidge RJ, Knight RA, Jiang Q. Mechanisms and predictive value of the decrease in water diffusion in cerebral ischemia. In: Le Bihan D, editor. Diffusion and Perfusion Magnetic Resonance Imaging: Applications to Functional MRI. New York: Raven Press; p. 173-80 (1995).

25. Mills R. Self-diffusion in normal and heavy water in the range 1-45°. J. Phys. Chem. 77(5), 685-8 (1973).

26. Duong TQ, Ackerman JJH, Ying HS & Neil JJ. Evaluation of Extra- and intracellular apparent diffusion in normal and globally ischaemic rat brain via ^{19}F NMR. Magn. Reson. Med. 40, 1-13 (1998).

27. Busza AL, Lythgoe MF, Allen KL, Williams SR. T2 decreases in acute global cerebral ischaemia in the Gerbil - the contribution of magnetic susceptibility gradients [Abstract]. In: "Proc., ISMRM, 2nd Annual Meeting, San Francisco, USA, 1994", p.1389.

28. Grohn OHJ, Lukkarinen JA, Oja JME, Ulatowski JA, Traystman RJ, Kauppinen RA. Non-invasive detection of cerebral hypoperfusion and reversible ischemia from reductions in the magnetic resonance imaging relaxation time T2. J. Cereb. Blood Flow Metab. 18, 911-20 (1998).

29. Calamante F, Lythgoe MF, Pell GS, Thomas DL, King MD, Busza AL, Sotak CH, Williams SR, Ordidge RJ, Gadian DG. Early changes in water diffusion, perfusion, T1 and T2 during focal cerebral ischaemia in the rat studied at 8.5T. Magn. Reson. Med. 41, 479-485 (1999).

30. Hsu EW, Aiken NR, Blackband SJ. Nuclear magnetic resonance microscopy of single neurons under hypotonic perturbation. Am. J. Physiol. 271: C1895-C1900 (1996)

31. Vajda Z, Berenyi E, Bogner P, Repa I, Doczi T, Sulyok E. Brain adaptation to water loading in rabbits as assessed by NMR relaxometry. Pediatric Res. 46, 450-454 (1999).

Figure legends

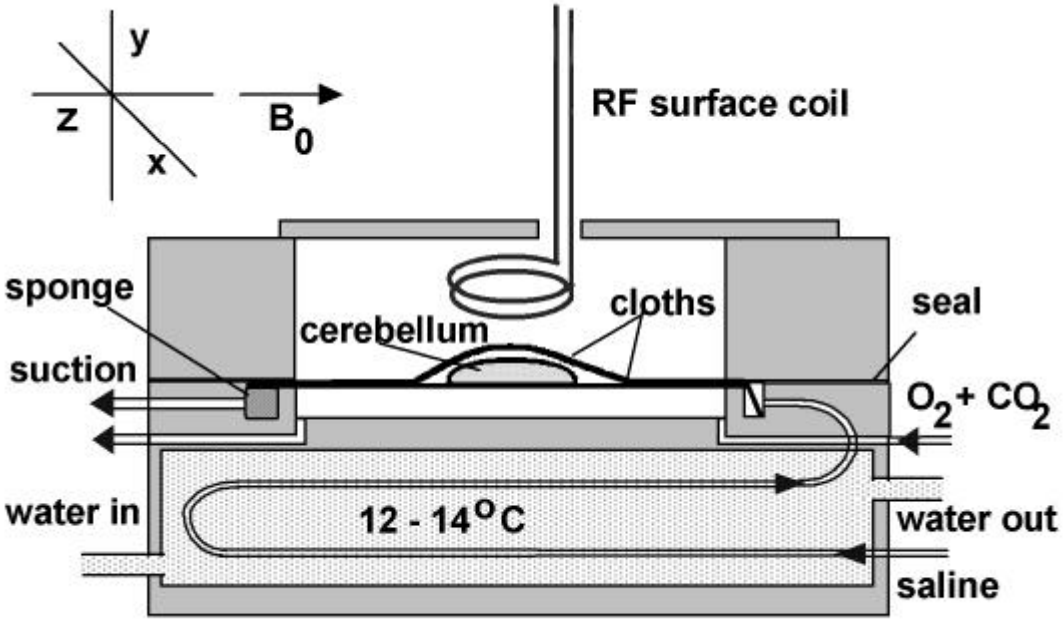

Fig. 1. The perfusion system in the magnet bore, made from perspex sealed with silicone rubber and nylon screws. Cooled saline flowed along a double layer of cloth enclosing the tissue, with O_2, CO_2 gas mixture above and below. The inner chamber was surrounded on three sides by circulating cold water (12-14 °C). The RF receiving coil (6mm dia.) was within 2mm of the tissue. The chamber was covered with a loosely fitting perspex lid.

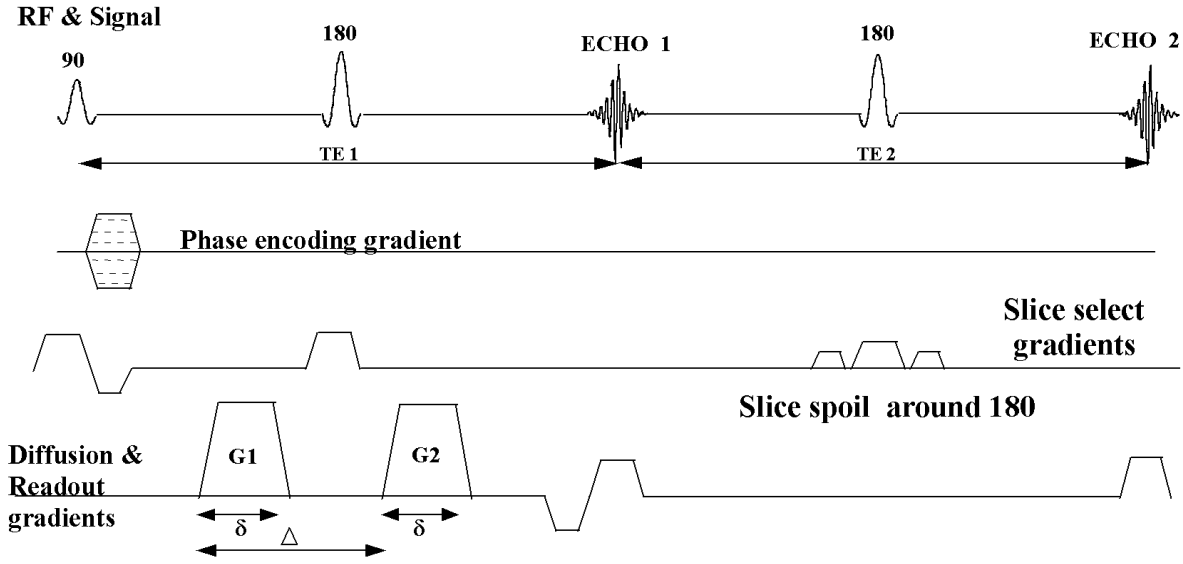

Fig. 2. Double echo sequence used to acquire images allowing calculation of ADC and apparent T2, at two echo times (TE = 80 ms, 160 ms). A diffusion weighted sequence is shown, with gradients applied around the first 180° pulse. These were interleaved with equivalent sequences in which these gradients were replaced with much smaller slice spoil

gradients.

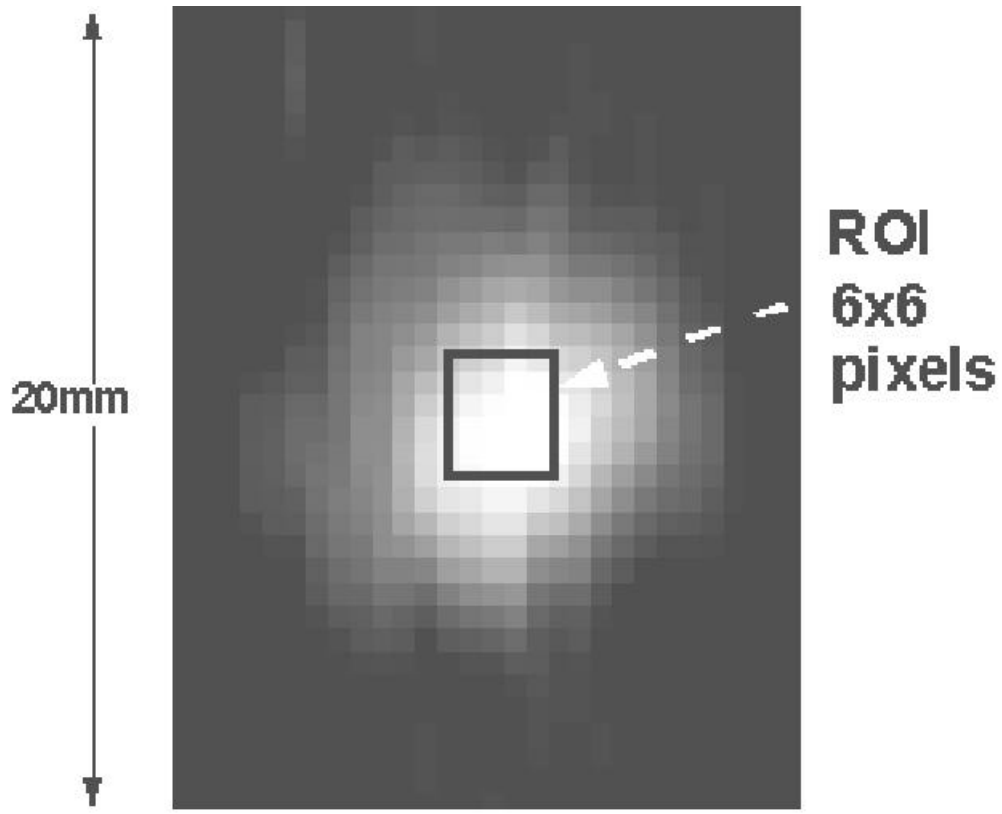

Fig. 3. Image of a cerebellum showing the ROI used for signal intensity measurement. The flow direction and principal field axis (Z: Fig.1) are vertical.

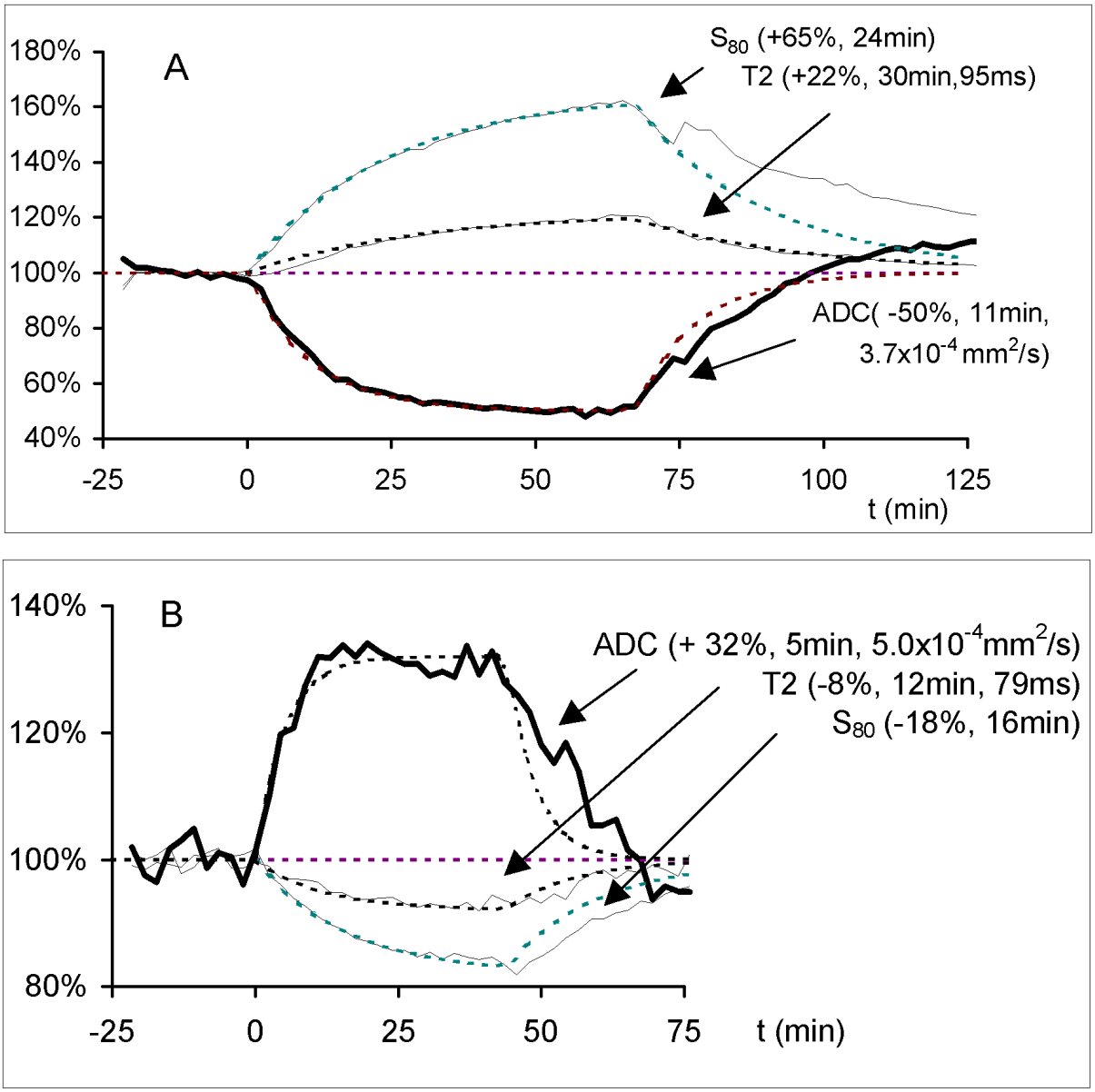

Fig. 4. Illustrative data from double-echo experiments in which preparations were exposed to (A) reduced osmolarity (170 mosmol.l^{-1}) for 65 min and (B) increased osmolarity (781 mosmol.l^{-1}) for 45 min. Signal Intensity (S_{80}) and the ADC and T2 calculated from equations 1 and 2 are shown as percentages of baseline values before the solution changes at time t=0. Exponential fits (dashed lines) with indicated amplitudes, exponential time constants and baseline values for ADC and T2 are shown for each graph, fitted up to the time of restoration of control solution; subsequent relaxation to baseline is shown with the same time constant, but not taken into account in the fit.

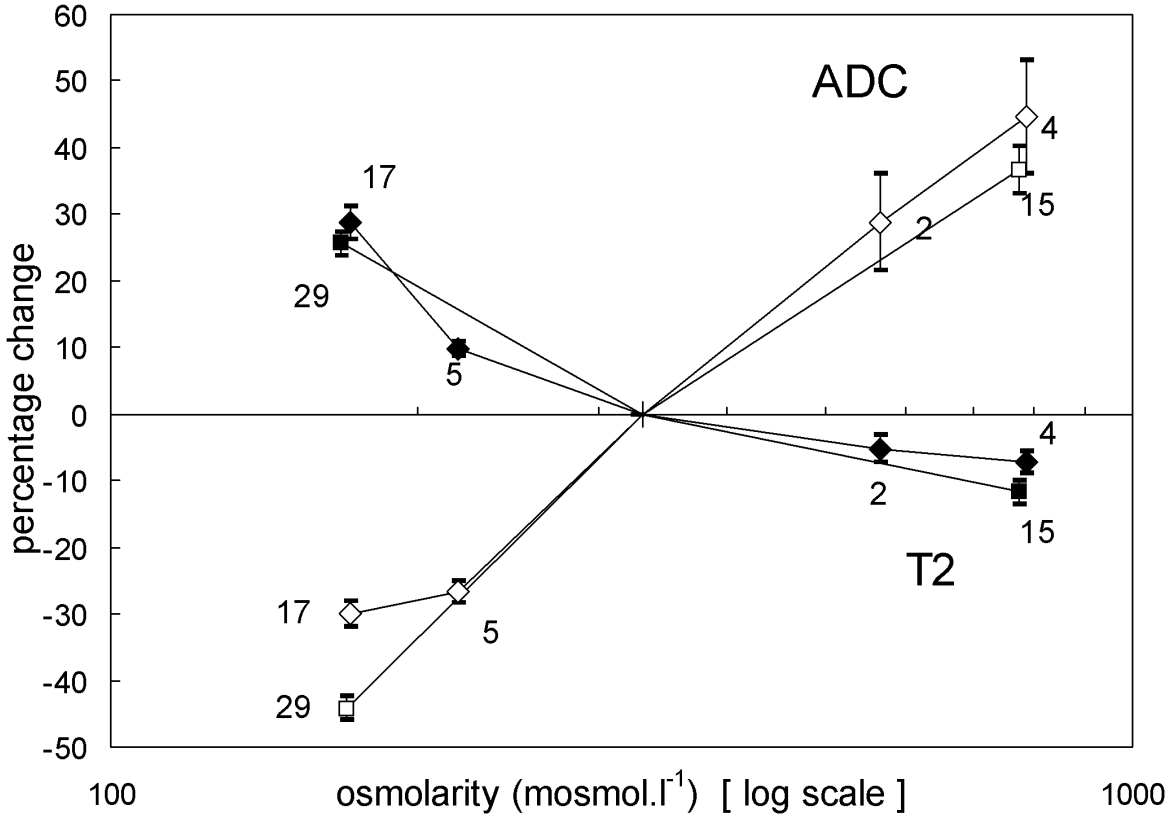

Fig. 5. Summary of changes in ADC and T2 in double echo experiments. Means (± 1 s.e.m., based on the indicated numbers of measurements) are shown for the percentage changes of ADC (open symbols, full lines) and T2 (filled symbols) in 2 sets of double-echo experiments in which diffusion gradients were along the x-axis in the plane of the tissue (squares, from 31 preparations) and the y-axis perpendicular to the tissue (diamonds, from 13 preparations). Overlapping points are slightly displaced laterally for clarity.

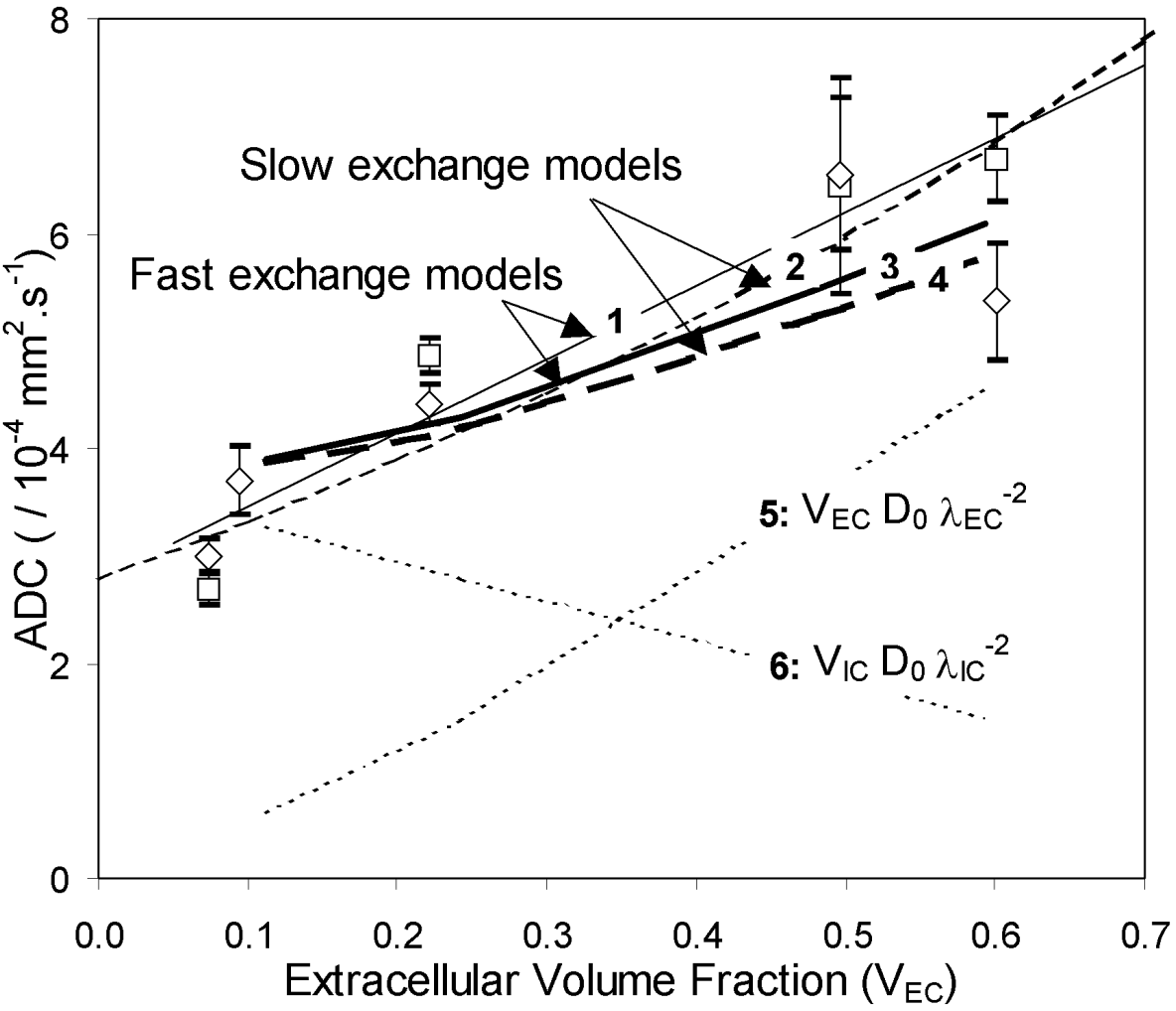

Fig. 6. ADC measurements related to the inferred extracellular volume fraction V_{EC} from data of Krizaj et al. (22) obtained under similar conditions. Data points are mean absolute ADC measurements (± s.e.m.) for the same experiments as Fig. 5, with diffusion gradients on the x-axis (squares) and y-axis (diamonds). Lines show fits to models with either fast (1,3: full lines) or slow (2,4: dashed lines) trans-membrane proton exchange. Models 1,2 assume constant EC and IC diffusivity with best-fit parameters (in units of 10^{-4} $mm^2.s^{-1}$): ADC_{EC} = 9.6, ADC_{IC} = 2.8 for fast exchange (equation 3) and ADC_{EC} = 11.0, ADC_{IC} = 2.8 for slow exchange (equation 5). Models 3,4 employ ADC_{EC} values inferred from measurements of V_{EC}, λ_{EC} made by Krizaj et al. (22) for EC ions, with D_o=17.2×10^{-4} $mm^2.s^{-1}$ and ADC_{IC} = 3.6 ×10^{-4} $mm^2.s^{-1}$ (λ_{IC} =2.2). Lines 5,6 show the separate EC and IC contributions to diffusion flux for models 3,4 as identified in Equation 3.